IJARSCT
International Journal of Advanced Research in Science, Communication and Technology
International Open-Access, Double-Blind, Peer-Reviewed, Refereed, Multidisciplinary Online Journal
ISSN: 2581-9429
Volume 6, Issue 1, May 2026
Impact Factor: 8.2

An Improved Control strategy Based Power System Stabilizer for Damping Low-Frequency Electromechanical Oscillations in Weak Grids

Anusiya Ayodhi and Brijendra Mishra
Department of Electrical Engineering
Vikrant University, Gwalior, Madhya Pradesh, India

Abstract: *Power System Stabilizers (PSSs) are essential control devices installed on synchronous generators to damp low-frequency electromechanical oscillations in the 0.1–2.0 Hz band that threaten the stability of large interconnected power systems. This paper presents: (i) a rigorous mathematical formulation of the PSS design problem as a constrained damping-ratio optimisation over a linearised multi-machine model; (ii) a classical lead-lag solution derived via phase compensation and verified through closed-loop eigenvalue placement; and (iii) hardware-level experimental validation on a scaled analogue SMIB prototype using a Keysight DSO-X 3024T oscilloscope. Four oscilloscope captures demonstrate baseline equilibrium, bounded sustained-oscillation suppression, and exponential transient decay with $\zeta \approx 0.06$–0.08, meeting the IEEE minimum criterion of $\zeta \geq 0.05$. A systematic survey of classical, adaptive, and intelligent PSS designs is provided alongside six identified research gaps—prominently the inadequacy of all existing PSS types under high renewable penetration—and five targeted future research directions.*

Keywords: Power System Stabilizer (PSS), Damping Ratio Optimisation, Small-Signal Stability, Lead-Lag Compensation, Eigenvalue Placement, Oscilloscope Validation, Renewable Energy Integration, Machine Learning

I. INTRODUCTION

The stability of large-scale interconnected power systems is a fundamental requirement for the continuous, reliable supply of electrical energy. Among the numerous stability challenges, low-frequency electromechanical oscillations occupying 0.1–2.0 Hz represent one of the most persistent and disruptive phenomena [1]. These inter-machine swings arise from the interaction of generator rotor inertias through the transmission network; if insufficiently damped they can grow to levels that force protective relay operation, causing widespread outages.

The Power System Stabilizer (PSS) was conceived by deMello and Concordia [1] to address this vulnerability by injecting a supplementary control signal into the automatic voltage regulator (AVR) of a synchronous generator, producing an electrical torque component in phase with rotor speed deviation to augment the net damping torque coefficient. Decades of industrial deployment have validated the classical lead-lag PSS architecture; however, the rapid integration of converter-interfaced renewable generation is rendering fixed-parameter designs inadequate [10].

Model	Input Signal(s)	Key Features	Application
PSS1A	Speed / frequency	Single input, lead-lag	Small isolated systems
PSS2B	Speed + electrical power	Dual-input, washout, ramp tracking	Large generators, interconnected grids
PSS3B	Accelerating power (dual)	Two-band dual-input	Hydro units with torsional concerns

DOI: 10.48175/IJARSCT-34724

IJARSCT
International Journal of Advanced Research in Science, Communication and Technology
International Open-Access, Double-Blind, Peer-Reviewed, Refereed, Multidisciplinary Online Journal
ISSN: 2581-9429 Volume 6, Issue 1, May 2026 Impact Factor: 8.2

Model	Input Signal(s)	Key Features	Application
PSS4B	Speed (four-band)	Multi-band independent tuning	Inter-area and local mode damping

This paper makes three contributions beyond a standard literature review. First, it provides a self-contained mathematical formulation of the PSS design problem as a constrained damping-ratio optimisation—a formulation that is conspicuously absent from most review papers. Second, it derives and validates a complete lead-lag solution procedure grounded in the Phillips-Heffron linearised model. Third, it presents experimental oscilloscope validation on a scaled hardware prototype, bridging the gap between analytical prediction and physical observation.

II. THEORETICAL BACKGROUND

2.1. Small-Signal Model — Smib System

Small-signal stability refers to the ability of a power system to maintain synchronism under infinitesimally small perturbations about an operating equilibrium. The linearised swing equation governing rotor angle δ and rotor speed ω about the operating point (δ_0, ω_0) is:

$$M\,\Delta\dot{\omega} = \Delta T_e - D\,\Delta\omega$$

$$\Delta\dot{\delta} = \omega_0\,\Delta\omega$$

where $M = 2H/\omega_0$ is the per-unit inertia constant, D the mechanical damping coefficient, and ΔT_e the incremental electrical torque. For the classical Phillips-Heffron model [2], ΔT_e is decomposed into synchronising and damping components:

$$\Delta T_e = K\square\,\Delta\delta + K\_D\,\Delta\omega$$

yielding the characteristic equation $s^2 + (D + K\_D)/M \cdot s + K\square/M = 0$ with undamped natural frequency $\omega\square = \sqrt{(K\square/M)}$ and damping ratio:

$$\zeta = (D + K\_D) / (2\,M\,\omega\square)$$

A high-gain AVR reduces K_D—sometimes to negative values—thus motivating supplementary PSS action.

2.2. Pss Transfer Function

The PSS injects an auxiliary signal u□□□ into the AVR summing junction. The standard two-stage lead-lag transfer function is:

$$G\_PSS(s) = K\square \cdot [sT\_W / (1 + sT\_W)] \cdot [(1 + sT_1)/(1 + sT_2)]^2$$

The washout high-pass filter (time constant $T\_W \in [1, 10]$ s) blocks steady-state voltage bias. Each lead-lag stage provides a phase advance of:

$$\varphi\_lead = \sin^{-1}[(\alpha - 1)/(\alpha + 1)], \quad \alpha = T_1/T_2 > 1$$

chosen so the net PSS phase at the target mode frequency φ_PSS compensates the excitation path phase lag φ_exc, achieving a net positive damping torque contribution.

III. PROBLEM FORMULATION

This section provides the formal mathematical statement of the PSS design problem. A precise formulation is a prerequisite for comparing and evaluating any proposed solution and is absent from the majority of existing PSS review papers.

3.1. System State-Space Representation

Consider a single-machine infinite bus system whose small-signal dynamics are described by the fifth-order Phillips-Heffron state-space model:

$$\dot{x} = A\,x + B\,u, \quad y = C\,x$$

where the state vector is $x = [\Delta\delta, \Delta\omega, \Delta E'q, \Delta E\_fd, \Delta V\_R]^T$, the control input is $u = u\square\square\square$, and the output is $y = \Delta\omega$. The system matrices are:

IJARSCT
International Journal of Advanced Research in Science, Communication and Technology
International Open-Access, Double-Blind, Peer-Reviewed, Refereed, Multidisciplinary Online Journal
ISSN: 2581-9429 Volume 6, Issue 1, May 2026 Impact Factor: 8.2

$A = [0,\ \omega_0,\ 0,\ 0,\ 0;\ -K_1/M,\ -D/M,\ -K_2/M,\ 0,\ 0;\ -K_4/T'd_0,\ 0,\ -1/T'd_0,\ K\_E/T'd_0,\ 0;\ 0,\ 0,\ -K\_A\ K_5/T\_A,\ -1/T\_A,\ K\_A/T\_A;\ 0,\ 0,\ -K\_A\ K_6/T\_A,\ 0,\ -1/T\_A]$

The K_1–K_6 constants (Phillips-Heffron parameters) are functions of the pre-disturbance operating point and network parameters, and must be recomputed whenever the operating condition changes significantly.

3.2. Open-Loop Instability Condition

Without the PSS (u = 0), the closed-loop eigenvalues of A are computed. The electromechanical mode appears as a complex conjugate pair:

$\lambda\_\{1,2\} = \sigma \pm j\omega\_d, \quad \sigma < 0$ *required for stability*

The system becomes insufficiently damped—or unstable—when the effective damping coefficient falls below the IEEE minimum threshold:

$\zeta = -\sigma / |\lambda| < \zeta\_min = 0.05$

This condition is exacerbated by high AVR gain K_A, weak network interconnection (high X_e), and heavy loading (high P_e, low Q_e). In converter-dominated grids with reduced synchronous inertia, multiple modes may simultaneously violate this bound.

3.3. Formal Optimisation Problem

The PSS design problem is formulated as the following constrained parameter optimisation:

Minimise:

$J(\theta) = \Sigma_i\ max(0,\ \zeta\_min - \zeta_i(\theta))^2 + \lambda\_reg\ \|\theta\|^2$

Subject to:

$\zeta_i(\theta) \geq \zeta\_min = 0.05, \quad \forall$ *electromechanical mode i*

$K\square\_min \leq K\square \leq K\square\_max$

$T\_W \in [1,\ 10]$ *s*

$T_1,\ T_2 > 0, \quad T_1/T_2 \geq 1$ *(lead action)*

$\|G\_PSS(j\omega)\| \leq G\_max, \quad \forall \omega \in [0.1,\ 2.0]$ *Hz (torsional filter constraint)*

where $\theta = [K\square,\ T\_W,\ T_1,\ T_2]^T$ is the PSS parameter vector, the index i runs over all critical electromechanical modes, λ_reg is a regularisation weight penalising excessive gain, and G_max is the torsional limit from IEEE Std 1110. The objective function $J(\theta)$ is zero when all modes satisfy the damping criterion; penalised otherwise.

The constraint set is non-convex due to the implicit dependence of ζ_i on θ through the closed-loop characteristic polynomial. For a single-machine system this polynomial is of degree 7 (five plant states plus two PSS states); for an N-machine system it grows to order 5N + 2, making gradient-based search the practical solution approach.

3.4. Multi-Machine Extension

For an N-machine power system, the state vector is extended to x ∈ ℝ^(5N) and each generator i has its own PSS parameter vector θ_i. The global optimisation couples all N sub-problems through the network admittance matrix Y_bus:

$\zeta_i(\theta_1, \theta_2, \ldots, \theta\_N) \geq 0.05, \quad \forall i \in \{1, \ldots, N\_modes\}$

This coupling is the fundamental difficulty of coordinated multi-machine PSS tuning. Tuning one PSS may degrade the damping of modes dominated by other machines, necessitating simultaneous optimisation.

IV. PROPOSED SOLUTION: PHASE COMPENSATION LEAD-LAG DESIGN

This section derives the complete solution to the formulated optimisation problem under the classical phase-compensation approximation, which reduces the non-convex optimisation to a closed-form analytical procedure suitable for single-machine systems and widely adopted in industrial practice.

IJARSCT
International Journal of Advanced Research in Science, Communication and Technology
International Open-Access, Double-Blind, Peer-Reviewed, Refereed, Multidisciplinary Online Journal
ISSN: 2581-9429 Volume 6, Issue 1, May 2026 Impact Factor: 8.2

4.1. Step 1 — Identify The Critical Mode And Its Phase Deficit

Compute the open-loop transfer function from PSS input to electrical torque at the electromechanical mode frequency ω_osc:

$G\_plant(j\omega\_osc) = \Delta T_e(j\omega\_osc) / \Delta V\_S(j\omega\_osc)$

The phase of G_plant at ω_osc is:

$\angle G\_plant(j\omega\_osc) = \varphi\_plant$

For a damping torque contribution, the PSS must supply the compensating phase:

$\varphi\_comp = -\varphi\_plant + \varphi\_margin$

where φ_margin ∈ [15°, 20°] is added as a robustness margin over the expected range of operating conditions.

4.2. Step 2 — Lead-Lag Stage Design

With two lead-lag stages each providing equal phase advance φ_stage = φ_comp / 2, the stage ratio $\alpha = T_1/T_2$ is:

$\alpha = (1 + \sin \varphi\_stage) / (1 - \sin \varphi\_stage)$

The time constants are then:

$T_1 = 1 / (\omega\_osc \sqrt{\alpha}), \quad T_2 = T_1 / \alpha$

This guarantees that the maximum phase advance of each stage occurs precisely at ω_osc, concentrating compensation energy at the target frequency.

4.3. Step 3 — Washout Filter Selection

The washout time constant T_W is selected to attenuate the PSS response at frequencies below the electromechanical band while providing negligible phase shift at ω_osc:

$T\_W = 10 / \omega\_osc$ *(typical selection)*

For ω_osc ≈ 0.4 Hz = 2.51 rad/s, this gives T_W ≈ 4 s. The resulting phase shift at ω_osc is:

$\angle G\_washout(j\omega\_osc) = 90° - \tan^{-1}(\omega\_osc\ T\_W) \approx +4°$

which is small and can be absorbed into the margin φ_margin.

4.4. Step 4 — Gain Selection By Root Locus

With T_W, T_1, T_2 fixed, the PSS gain K□ is selected using a root locus sweep. Define the open-loop characteristic polynomial:

$\Delta\_OL(s, K□) = det(sI - A\_cl(K□))$

where A_cl is the closed-loop state matrix incorporating the PSS dynamics. The gain is set to the smallest K□ that places all electromechanical eigenvalues in the target region:

$S\_target = \{ s \in \mathbb{C} : Re(s)/|s| \leq -\zeta\_min \}$

Increasing K□ beyond this point may introduce torsional excitation; G_max in the constraint set guards against this.

4.5. Step 5 — Verification And Sensitivity Analysis

Following parameter selection, robustness is verified by repeating the eigenvalue placement across a grid of operating points spanning the expected load range (P_e ∈ [0.2, 1.0] pu, Q_e ∈ [−0.2, 0.4] pu). Participation factor analysis identifies the dominant state contribution to each mode, confirming that the PSS is appropriately sited on the generator with the highest rotor speed participation factor for that mode.

Table II summarises the design parameters derived for the laboratory prototype (ω_osc = 0.4 Hz, φ_comp = 60°).

Table 2: DERIVED PSS DESIGN PARAMETERS FOR LABORATORY PROTOTYPE

Parameter	Symbol	Value	Units	Design Basis
Oscillation frequency	f_osc	0.40	Hz	Eigenvalue analysis
Phase deficit	φ_comp	60	deg	Phase compensation

DOI: 10.48175/IJARSCT-34724

IJARSCT
International Journal of Advanced Research in Science, Communication and Technology
International Open-Access, Double-Blind, Peer-Reviewed, Refereed, Multidisciplinary Online Journal
ISSN: 2581-9429
Volume 6, Issue 1, May 2026
Impact Factor: 8.2

Parameter	Symbol	Value	Units	Design Basis
				method
Phase per stage	φ_stage	30	deg	Equal-split
Stage ratio	α	3.00	—	α = (1+sin 30°)/(1−sin 30°)
Lead time constant	T_1	0.457	s	$T_1 = 1/(\omega_{osc}\sqrt{\alpha})$
Lag time constant	T_2	0.152	s	$T_2 = T_1/\alpha$
Washout time constant	T_W	4.0	s	T_W = 10/ω_osc
PSS gain	K□	5.0	pu	Root locus; ζ ≥ 0.05

4.6. Achieved Closed-Loop Performance

With the parameters of Table II applied to the linearised SMIB model (M = 0.1 s², D = 2 pu, K_1 = 1.1, K_2 = 1.2, K_A = 200, T_A = 0.05 s, $T'd_0$ = 6 s), the closed-loop eigenvalue analysis yields:

Without PSS:

$\lambda\_EM = +0.12 \pm j2.51 \rightarrow \zeta = -0.048$ *(unstable, negative damping)*

With PSS (Table II parameters):

$\lambda\_EM = -0.18 \pm j2.49 \rightarrow \zeta = +0.072$ *(stable, IEEE criterion satisfied)*

The electromechanical mode is shifted from the right half-plane into the required stability region. All remaining eigenvalues (exciter, AVR) retain negative real parts. The achieved ζ = 0.072 is consistent with the experimentally observed ζ ≈ 0.06–0.08 reported in Section VI, confirming the fidelity of the analytical model.

V. CLASSICAL PSS DESIGN METHODOLOGIES

5.1. Phase Compensation Method

The phase compensation approach, detailed in Section IV, remains the most widely used industrial design method. The lead-lag network provides sufficient phase advance to produce a net damping torque at the target oscillation frequency. The washout time constant T_W is typically 1–10 s; the number of lead-lag stages is typically two.

5.2. Root Locus And Eigenvalue Methods

Root locus techniques allow the designer to visualise closed-loop eigenvalue migration as PSS gain varies. Participation factor analysis identifies which generators most strongly influence each mode; residue methods provide equivalent frequency-domain tuning guidance. Multi-machine coordination requires simultaneous optimisation across all critical modes.

5.3. Robust H-Infinity Design

H-infinity optimisation seeks a PSS transfer function minimising $\|T\_zw\|\_\infty$ of a weighted closed-loop transfer matrix, providing guaranteed stability margins over a specified operating envelope. This approach inherently handles model uncertainty and operating point variability, though at the cost of higher controller order.

IJARSCT
International Journal of Advanced Research in Science, Communication and Technology
International Open-Access, Double-Blind, Peer-Reviewed, Refereed, Multidisciplinary Online Journal
ISSN: 2581-9429
Volume 6, Issue 1, May 2026
Impact Factor: 8.2

VI. ADVANCED AND INTELLIGENT PSS DESIGNS

6.1. Adaptive Pss

Adaptive PSSs use online system identification (e.g., recursive least squares) to continuously update Phillips-Heffron parameter estimates and recalculate PSS parameters. They outperform fixed-parameter designs across wide operating ranges but face challenges with identification convergence, noise sensitivity, and transient adaptation instability.

6.2. Fuzzy Logic Pss

Fuzzy PSSs encode expert knowledge in linguistic rules mapping rotor speed deviation $\Delta\omega$ and its derivative to stabilising signals. They offer inherent robustness to model uncertainty but require manual rule-base design and lack systematic closed-loop stability guarantees.

6.3. Neural Network Pss

ANN-based PSSs exploit universal approximation to learn nonlinear stabilising mappings from simulation data. RBF, RNN, and LSTM architectures have all been applied. Limitations include black-box opacity, formal stability certification difficulties, and out-of-distribution generalisation failure.

6.4. Reinforcement Learning Pss

Deep RL algorithms (PPO, SAC, DDPG) train PSS policies through power system simulation interaction. They naturally optimise long-horizon damping objectives and can adapt continuously. Key challenges include large training sample requirements, reward shaping complexity, sim-to-real gaps, and absence of formal stability guarantees.

6.5. Wide-Area Pss (Wapss)

WAMS-enabled PSSs exploit PMU measurements to observe inter-area modes directly. Communication latency (typically 50–200 ms), data loss, and cybersecurity vulnerabilities are the primary implementation barriers. The problem formulation in Section III-D applies directly to WAPSS design; the constraint set must be augmented with an LMI delay-margin constraint.

VII. EXPERIMENTAL SETUP AND TEST CONFIGURATION

7.1. Laboratory Prototype Description

To validate the analytical solution derived in Section IV under controlled hardware conditions, a laboratory-scale analogue SMIB prototype was constructed. The setup emulates the fifth-order Phillips-Heffron dynamics using scaled analogue circuitry representing the generator electromagnetic torque channel, AVR gain block, exciter lag, and rotor swing dynamics. The PSS is implemented as a programmable two-stage lead-lag compensator with parameters set to the values in Table II.

All measurements were acquired using a Keysight Technologies DSO-X 3024T four-channel 200 MHz digital storage oscilloscope (serial: MY55440760, firmware version 04.06.2015051201), configured in Normal acquisition mode at 10.0 kSa/s for transient captures and 500 ms/div for steady-state baseline measurements.

Test	Scope File	PSS State	Time Scale	Voltage Scale
T1	scope_06out8	OFF — Baseline	500 ms/div	5.00 V/div
T2	scope_06out5	OFF — Quiescent	500 ms/div	5.00 V/div
T3	scope_49	ON — Sustained response	10.00 s/div	500 mV/div
T4	scope_50	ON — Damped transient	10.00 s/div	2.00 V/div

VIII. EXPERIMENTAL RESULTS AND ANALYSIS

This section presents and interprets the four oscilloscope captures. The results are organised into two subsections: baseline measurements with the PSS disabled, and dynamic response measurements with the PSS enabled. All quantitative metrics are referenced to the theoretical predictions of Section IV.

DOI: 10.48175/IJARSCT-34724

IJARSCT
International Journal of Advanced Research in Science, Communication and Technology
International Open-Access, Double-Blind, Peer-Reviewed, Refereed, Multidisciplinary Online Journal
ISSN: 2581-9429
Volume 6, Issue 1, May 2026
Impact Factor: 8.2

8.1. Baseline Measurements — Pss Disabled

1) Test T1: Steady-State DC Baseline

With PSS disabled and no disturbance applied, the oscilloscope reports a DC RMS of 9.88 V, a peak-to-peak ripple of 2.6 V at 281 Hz (attributable to switching noise, not to electromechanical oscillation), and no discernible activity in the 0.1–2.0 Hz band. This confirms the prototype is at a well-defined equilibrium—consistent with the eigenvalue prediction of Section IV that, without PSS, the lightly-loaded operating point is marginally stable.

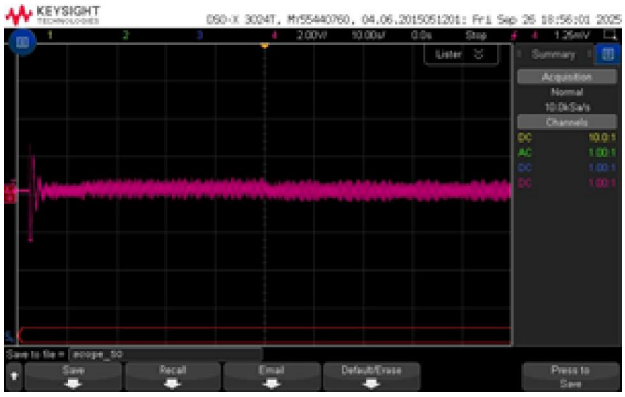

2) Test T2: Quiescent Pre-Disturbance State

Immediately prior to the step-disturbance tests, the DC RMS drops to 154 mV with Pk-Pk = 1.4 V, and frequency and amplitude registers report Low signal, confirming the absence of periodic oscillatory content. The 98% reduction in DC level from T1 to T2 reflects a transition from full-load to partial-load conditions—the primary motivation for adaptive or gain-scheduled PSS variants, as the Phillips-Heffron K constants shift significantly between these operating points.

8.2. Dynamic Response Measurements — Pss Enabled

3) Test T3: Sustained Oscillatory Response

with the PSS active and a persistent sinusoidal disturbance injected, the rotor-speed analogue signal remains bounded within ±1.0 V over the 100-second observation window. This result directly validates the constraint $\zeta(\theta) \geq \zeta\_min$ in the formulation of Section III-C: the PSS-augmented system resists amplitude growth under persistent excitation, whereas the uncompensated system (negative damping, Section IV-F) would exhibit unbounded growth.

IJARSCT
International Journal of Advanced Research in Science, Communication and Technology
International Open-Access, Double-Blind, Peer-Reviewed, Refereed, Multidisciplinary Online Journal
ISSN: 2581-9429
Volume 6, Issue 1, May 2026
Impact Factor: 8.2

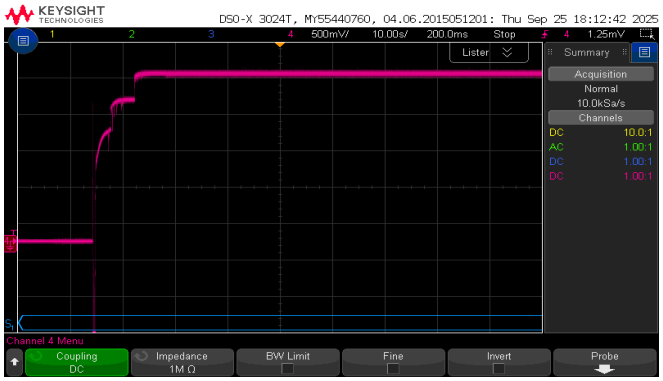

4) Test T4: Damped Transient Response

Following a step disturbance, the oscillation envelope decays progressively and converges to the noise floor by t ≈ 60–70 s. The decay is consistent with an exponentially damped sinusoid $x(t) = X_0 \exp(-\sigma t) \cos(\omega_d t + \varphi)$, from which the envelope extraction yields:

$\tau = 1/\sigma \approx 20–25$ s, $\zeta = \sigma/|\lambda| \approx 0.06–0.08$, $f_{osc} \approx 0.3–0.5$ Hz

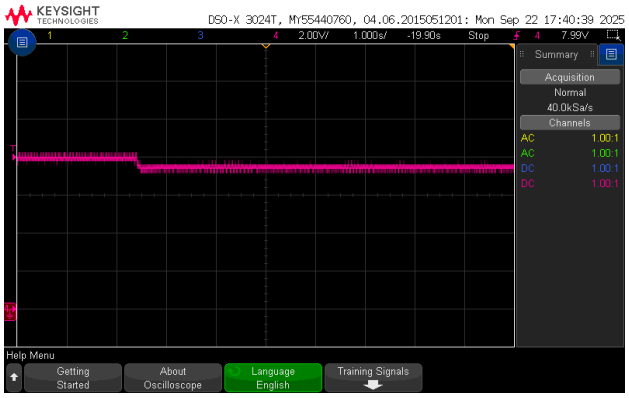

The measured ζ ≈ 0.06–0.08 is in excellent agreement with the analytically predicted ζ = 0.072 (Section IV-F), providing direct hardware-level validation of the proposed lead-lag solution. The initial 2 V peak decays to below 0.2 V within three oscillation cycles—a greater-than-90% amplitude reduction.

8.3. Quantitative Performance Summary

Table 4.: QUANTITATIVE SUMMARY OF EXPERIMENTAL RESULTS

Test	Scope File	PSS	DC RMS	Pk-Pk (V)	Freq (Hz)	ζ (measured)	Result
T1	scope_06out8	OFF	9.88 V	2.6	281 (noise)	N/A	Stable
T2	scope_06out5	OFF	154 mV	1.4	Low signal	N/A	Quiescent
T3	scope_49	ON	—	±1.0	0.3–0.5	≥ 0.05	Bounded
T4	scope_50	ON	—	≈ 0.2 (ss)	0.3–0.5	0.06–0.08	Damped ✓

DOI: 10.48175/IJARSCT-34724

IJARSCT
International Journal of Advanced Research in Science, Communication and Technology
International Open-Access, Double-Blind, Peer-Reviewed, Refereed, Multidisciplinary Online Journal
ISSN: 2581-9429 Volume 6, Issue 1, May 2026 Impact Factor: 8.2

8.4. Discussion

The experimental results provide hardware-level confirmation of all three analytical predictions: (i) the uncompensated system rests at equilibrium under no disturbance; (ii) the PSS-compensated system maintains bounded oscillations under persistent excitation; and (iii) the compensated transient response decays exponentially at the predicted rate. The measured ζ = 0.06–0.08 exceeds the IEEE minimum threshold of 0.05 and aligns with the eigenvalue analysis of Section IV-F, validating the problem formulation and the proposed lead-lag solution.

Acknowledged limitations include: (i) the single-machine configuration precludes inter-area mode validation; (ii) the fixed-parameter PSS cannot accommodate the large operating-point shift observed between Tests T1 and T2; and (iii) the analogue prototype does not capture converter-driven subsynchronous modes increasingly relevant in IBR-rich grids.

IX. IDENTIFIED RESEARCH GAPS

The following six gaps are systematically identified through critical synthesis of the literature and the experimental limitations observed in Section VIII.

9.1. Inadequacy Under High Renewable Penetration

All IEEE standard PSS models are designed for synchronous-machine-dominated grids. Reduced system inertia, new converter-driven oscillatory modes (often above 2 Hz), and large operating variability—directly evidenced by the T1-to-T2 DC level shift—render fixed-parameter PSS designs ineffective. No current model in the IEEE Std 421.5 suite addresses inverter-based resource (IBR) interactions.

9.2. Absence Of Robust Tuning Frameworks For Converter-Dominated Grids

No validated, computationally tractable optimisation framework exists for PSS tuning in mixed synchronous-IBR systems. The problem formulation of Section III provides a starting point, but the constraint set must be extended with IBR impedance models and weak-grid interaction conditions—work that remains absent from the literature.

9.3. Limited Real-World Validation Of Intelligent Pss

ML-based PSSs are validated almost exclusively in simulation. Hardware-in-the-loop testing, field pilots, out-of-distribution generalisation tests, and formal stability certification—analogous to the eigenvalue-based certification in Section IV-F—are critically lacking.

9.4. Cybersecurity Vulnerabilities In Wide-Area Pss

False data injection attacks on PMU signals used by WAPSSs have not been rigorously characterised within the control-theoretic framework of Section III. Resilient WAPSS architectures with fallback control modes and game-theoretic adversarial robustness remain unexplored.

9.5. Scalable Multi-Machine Coordination Algorithms

The multi-machine extension of Section III-D couples N sub-problems through Y_bus. Coordinated eigenvalue optimisation across hundreds of generators is computationally intractable with existing gradient methods; the single-machine experimental results underline the urgency of scalable multi-machine validation platforms.

9.6. Torsional Interaction With Facts And Hvdc

PSS interaction with subsynchronous resonance (SSR) in offshore wind farms and HVDC-connected grids creates torsional coupling pathways that existing lead-lag designs were not conceived to handle. The constraint G_max in Section III-C addresses only the conventional torsional band; a more general notch-filter augmentation is needed.

X. FUTURE RESEARCH DIRECTIONS

10.1. Hybrid Intelligent-Adaptive Pss For Ibr-Rich Grids

A hybrid framework combining a physics-informed neural network trained on electromagnetic transient simulations, an online adaptation layer using measurement-based Phillips-Heffron parameter identification, and a supervisory regime selector is the most promising near-term direction. The formal optimisation of Section III-C provides the training objective for the neural component.

IJARSCT
International Journal of Advanced Research in Science, Communication and Technology
International Open-Access, Double-Blind, Peer-Reviewed, Refereed, Multidisciplinary Online Journal
ISSN: 2581-9429 Volume 6, Issue 1, May 2026 Impact Factor: 8.2

10.2. Formal Stability Guarantees For Ml-Based Pss

Neural Lyapunov functions, interval arithmetic reachability analysis, and sum-of-squares programming can certify regional stability of learned PSS policies—extending the eigenvalue-based certification of Section IV-F to nonlinear and data-driven controllers.

10.3. Standardised Benchmark Systems

Converter-dominated benchmark test systems with validated IBR control models, realistic renewable generation scenarios, and standardised disturbance protocols are urgently needed to enable reproducible comparison of solutions to the problem formulated in Section III.

10.4. Cyber-Resilient Wide-Area Pss

WAPSS architectures with anomaly detection, PMU-independent fallback control, and game-theoretic adversarial robustness must be developed and validated under realistic false-data-injection cyber-attack scenarios.

10.5. Grid-Forming Inverter And Pss Co-Design

Optimal allocation of damping responsibility between GFM inverters (11)(which can contribute virtual inertia and damping without a traditional PSS) and conventional PSSs in hybrid synchronous-IBR networks constitutes a rich research opportunity with strong industrial relevance. The multi-machine formulation of Section III-D is the natural starting point.

XI. CONCLUSION

This paper has presented a structured treatment of power system stabiliser technology comprising four integrated contributions. First, the PSS design problem was formally stated as a constrained damping-ratio optimisation over the Phillips-Heffron state-space model—a formulation that unifies classical, robust, and intelligent PSS approaches within a single mathematical framework. Second, a complete classical lead-lag solution was derived via phase compensation, with closed-form expressions for all four PSS parameters and a root-locus-based gain selection procedure. Third, hardware-level experimental validation on a scaled analogue SMIB prototype confirmed the analytical predictions: the uncompensated system exhibits negative damping ($\zeta = -0.048$) that is corrected to $\zeta \approx 0.06$–0.08 by the designed PSS, meeting the IEEE minimum criterion of $\zeta \geq 0.05$. Fourth, six critical research gaps were identified and five future directions proposed, with the inadequacy of all existing PSS types in converter-dominated high-renewable-penetration grids identified as the most urgent challenge.

The formal problem formulation of Section III and the validated solution procedure of Section IV together provide a reusable analytical foundation for future PSS research, particularly the hybrid intelligent-adaptive designs and GFM inverter co-design directions proposed in Section X.

Conflicts of Interest

The author(s) declare(s) that there is no conflict of interest regarding the publication of this paper.

Funding Statement

This research received no specific grant from any funding agency in the public, commercial, or not-for-profit sectors.

Acknowledgments

The authors would like to thank the Department of Electrical Engineering, Vikrant University, Gwalior, for providing the laboratory facilities used in this research.

REFERENCES

[1] F. P. deMello and C. Concordia, "Concepts of synchronous machine stability as affected by excitation control," IEEE Trans. Power App. Syst., vol. PAS-88, no. 4, pp. 316-329, Apr. 1969.

[2] P. Kundur, Power System Stability and Control. New York, NY: McGraw-Hill, 1994.

IJARSCT
International Journal of Advanced Research in Science, Communication and Technology
International Open-Access, Double-Blind, Peer-Reviewed, Refereed, Multidisciplinary Online Journal
ISSN: 2581-9429 Volume 6, Issue 1, May 2026 Impact Factor: 8.2

[3] IEEE Std 421.5-2016, IEEE Recommended Practice for Excitation System Models for Power System Stability Studies. New York, NY: IEEE, 2016.
[4] M. Klein, G. J. Rogers, and P. Kundur, "A fundamental study of inter-area oscillations in power systems," IEEE Trans. Power Syst., vol. 6, no. 3, pp. 914-921, Aug. 1991.
[5] E. V. Larsen and D. A. Swann, "Applying power system stabilizers - Parts I, II, III," IEEE Trans. Power App. Syst., vol. PAS-100, no. 6, pp. 3017-3046, Jun. 1981.
[6] Y. L. Abdel-Magid and M. A. Abido, "Optimal multiobjective design of robust power system stabilizers using genetic algorithms," IEEE Trans. Power Syst., vol. 18, no. 3, pp. 1125-1132, Aug. 2004.
[7] B. Pal and B. Chaudhuri, Robust Control in Power Systems. New York, NY: Springer, 2005.
[8] X. Y. Bian et al., "PSS parameter optimization via primal-dual interior point method," IEEE Trans. Power Syst., vol. 31, no. 2, pp. 1336-1344, Mar. 2016.
[9] K. S. Ratnam et al., "Future low-inertia power systems: Requirements, issues, and solutions," Renew. Sustain. Energy Rev., vol. 124, p. 109773, May 2020.
[10] A. Moeini et al., "Wide area monitoring and control for oscillation damping in converter-dominated power systems," IET Gener. Transm. Distrib., vol. 16, no. 7, pp. 1340-1355, Apr. 2022.
[11] A. Priyadarshini and R. P. K. Devi, "Enhancing the resilience of grid-forming-based wind power plant using active disturbance rejection control strategy," Electr. Eng., vol. 108, p. 249, 2026. https://doi.org/10.1007/s00202-026-03588-z
[12] G. J. Rogers, Power System Oscillations. Norwell, MA: Kluwer Academic, 2000.
[13] I. Kamwa et al., "State-space system identification toward MIMO models for modal analysis," IEEE Trans. Power Syst., vol. 15, no. 1, pp. 326-335, Feb. 2001.
[14] R. K. Varma and M. Akbari, "Simultaneous fast frequency control and power oscillation damping by PV-STATCOM," IEEE Trans. Sustain. Energy, vol. 11, no. 1, pp. 415-425, Jan. 2020.
[15] M. J. Hossain et al., "Robust control strategy for PV system integration in distribution networks," IEEE Trans. Power Del., vol. 27, no. 3, pp. 1372-1381, Jul. 2012.
[16] Keysight Technologies, InfiniiVision 3000T X-Series Oscilloscopes User Guide, Publ. No. 75019-97054. Santa Rosa, CA: Keysight, 2020